Urban Climate 24 (2018) 1–18

Contents lists available at ScienceDirect

Urban Climate

journal homepage: www.elsevier.com/locate/uclim

Characterization of thermal environment over heterogeneous surface of National Capital Region (NCR), India using LANDSAT-8 sensor for regional planning studies

Hoang Thi Hang*, Atiqur Rahman

Department of Geography, Jamia Millia Islamia, New Delhi, India

ARTICLE INFO

Keywords:
Land surface temperature
Emissivity
Landsat 8
Mono-window algorithm
NDVI
NCR-India

ABSTRACT

Land surface temperature (LST) is an essential indicator of the Earth's surface energy budget. It is essential for urban micro-climate change studies and acts as a controlling variable in climatic models. The present study, LST retrieves with the improved mono-window algorithm from the Landsat-8 Thermal Infrared Sensor Band 10. The proportion of vegetation cover coupled with Normalized Difference Vegetation Index (NDVI) used for the estimation of emissivity. The derived emissivity and surface temperature over different ground features have compared with field observation as well as those in the literature and found in an accepted range (error of around 1–2%). Herein, results show that the spatial distribution of surface temperature was significantly affected by landscape characteristics. The built-up and commercial/industrial areas display higher surface temperature in comparison with surrounding other vegetated lands. Whereas, the cooling effect towards the surrounding urban built-up area are found increasing in the vegetated area, and inside the green zones. A strong correlation is observed between the LST with NDVI over different land cover and land use (LCLU) classes. The Geoinformation technique provides a practical-based theoretical model of the land characterization of an urban thermal environment which assists in regional planning and decision-making process.

1. Introduction

With the rapid urbanization and widespread urban sprawl have depleted vegetated cover and have increased vulnerability to micro-climate change in urban areas. It became increasingly severe problems in the semi-arid climatic zone (Koppen Geiger: BSh) specifically National Capital Region (NCR), India (Mallick et al., 2008; Yogesh et al., 2009; Suzanchi and Ravinder, 2011; Mallick et al., 2013). In hot semi-arid climates the NCR experiences, long summer, hot and dry climate. The neighbourhood micro-climate at the micro-scale closely relates to people's daily life (Roth, 2002). It is thus essential and necessary to study the urban climate and the neighbourhood microclimate in the hot semi-arid region for improving environmental quality, reducing building energy consumption and mitigating urban thermal environment for better quality of life.

Land surface temperature (LST) can be an essential source of information about the energy budget and climate, plays an essential role in many environmental and biophysical processes (Dousset and Gourmelon, 2003; Weng et al., 2004; Mallick et al., 2008). Previous studies have evaluated the relative temperature of urban settings by measuring the air temperature, using site-based measurement stations. Several researchers observing the temperature using infrared thermal sensors mounted on a vehicle, along with specified route (Yamashita et al., 1996). This technique is time-consuming and expensive and increases the problems in spatial

* Corresponding author.
E-mail address: hlhangstac@gmail.com (H.T. Hang).

https://doi.org/10.1016/j.uclim.2018.01.001
Received 25 October 2017; Received in revised form 5 January 2018; Accepted 8 January 2018
2212-0955/ © 2018 Elsevier B.V. All rights reserved.

analysis and interpolation. Satellite-based remote sensing techniques could be an enhanced alternative to retrieve the LST and other biophysical parameters. In the remote sensing technique, optical and thermal infrared (TIR) sensors have been used to acquire quantitative information on biophysical parameters and surface temperature respectively across the landscape.

Urbanization is creating massive transformation in land cover thereby modify the sensible and latent heat fluxes of the surface. Concrete Impervious surface areas have higher sensible heat in respect to vegetated areas, resulting in higher temperatures of urban built-up surfaces on the contrary to vegetated lands (Liu et al., 2012; Rahman et al., 2011). With this geographic phenomenon of thermal environment, other anthropogenic activities such as increased pollutant emission (Ali and Nitivattananon, 2012), population density (Mallick and Rahman, 2012) and others change the environment at local to regional scales (Grimm et al., 2008).

Due to their relevance to regional climate, quality life, urban air quality, land cover/land use (LCLU) change and carbon emission urban environment studied extensively worldwide over the last two decades viz. Shanghai (Chow, 1992), Tokya (Saitoh et al., 1996), Mexico City (Jauregui, 1997), Houston (Streutker, 2003), Indianapolis (Lu and Weng, 2006), Salt lake valley (Gluch et al., 2006), London (Jones and Lister, 2009), Tabriz (Amiri et al., 2009), Greater Athens (Keramitsoglou et al., 2011), Lahore (Ali and Nitivattananon, 2012), Dhaka (Molla et al., 2012), Wisconsin (Deng and Wu, 2013), Faislabad (Ali et al., 2012; Shabana et al., 2015) and Bangkok (Ali et al., 2017). In the Indian scenario, research on the urban thermal environment given more emphasis during the last decade (Mallick et al., 2008; Pandey et al., 2012; Chakraborty et al., 2013; Mallick et al., 2013; Mathew et al., 2016). However, the researchers investigated urban environment and Normalized Difference Vegetation Index (NDVI) relationship for major cities around the developed world. There is a gap of the research related to the large regions that comprise many cities of India. Problem statement concerning to land surface emissivity, LST and NDVI are explored by Mallick et al., 2008, Kant et al., 2009, Mallick et al., 2012, Sharma and Joshi, 2013a, 2013b for Delhi, while an urban thermal environment for NCR, India as a whole is still unexplored. Moreover, the rapid expansion of urbanization in NCR, India (Sharma and Joshi, 2016) during the last few decades has driven researchers to examine the urban thermal environment effects from an entirely new perspective in recent years.

In this study, LST retrieves with the improved mono-window algorithm from the Landsat-8 Thermal Infrared Sensor Band 10 and the proportion of vegetation cover coupled with Normalized Difference Vegetation Index (NDVI) used for the estimation of land surface emissivity (LSE) of NCR, India. The various studies of the ground emissivity databases (Salisbury and Daria, 1992) opted from laboratory measurements, and it represents the site-observation rather than the per-pixel spatial observation. Hence, the surface emissivity parameter per pixel needs to be derived from satellite pixel scale (30×30 m of Landsat-8 in this case) to have an accurate estimation of LST and assessment of other biophysical parameters. The study includes the assessment of the spatial variations of LST over different LCLU, relationship with vegetation cover. It also investigates the relationship between urban development, the ground-based measurements, satellite-derived land surface temperatures. The Geoinformation technique provides a practical-based theoretical model of the land characterization of an urban thermal environment which assists in regional planning and decision-making process.

2. Database and methodology

2.1. Study area: NCR, India

The National Capital Region (NCR) in India is a metropolitan area which consists of National Capital Territory (NCT) of Delhi, as well as urban areas surrounding it in neighbouring states of Haryana, Uttar Pradesh, and Rajasthan. National Capital Region (NCR) having a total area of 46,208 km^2 extending over 18 districts of Uttar Pradesh, Haryana, and Rajasthan and NCT of Delhi and constitutes about 1.60% of the country's land area.

In the NCR region, Delhi, the capital city of India, is the second most populated megacity in the world with nearly 17 million people with an area of 1483 km^2. Population in Delhi has increased from 1.7 million in 1951 to 13 million in 2001, finally crossing the mark of 16.7 million in 2011 (Census of India, 2011), as one of the high spread of suburban area in history (United Nations, 2012). This unprecedented growth has attracted a broad community of scientists and researchers to analyse the complex LCLU of Delhi (Sokhi et al., 1989; Punia et al., 2011; Wentz Elizabeth et al., 2008; Rahman et al., 2011; Mallick et al., 2013). In 1991, the urban core of Delhi was expanded to nearby interstate city areas such as Ghaziabad, Meerut, and Noida of Uttar Pradesh and Faridabad and Gurgaon of Haryana forming the National Capital Region (Fig. 1). Following this elevated status, this region has experienced rapid spatial changes in its landscape patterns. These changes, whether conversion of agricultural land to industry and civic facilities or sparse built-up areas to dense built-up areas have impacted the residential patterns, agricultural practices, urban thermal environment and urban forest distribution in the city. NCR, Delhi is characterized by highly complex land use practices with impervious concrete surfaces dominating the commercial, industrial as well as residential areas; and patches of forests at the heart of the city, in the north and the south. Peri-urban areas and banks of Yamuna River are predominantly covered with agricultural lands. Such high heterogeneity of land use provides high dynamism of land transformations over both long-term as well as short-term scales. The region has a tropical steppe climate. The general prevalence of continental air leads to relatively dry conditions with sweltering summers. Mean monthly temperatures range from 14 °C in January (min. 3 °C) to 35 °C in June (max. 47 °C). The NCR, Delhi experiences five significant seasons; winter (Nov–Feb), spring (Feb–Mar), summer (Apr–Jun), Monsoon (Jul–Sep), and Post-monsoon (Oct–early Nov).

2.2. Database

Landsat-8 is one of the most helpful satellite data for environmental and ecological studies. There are two new sensors on Landsat-

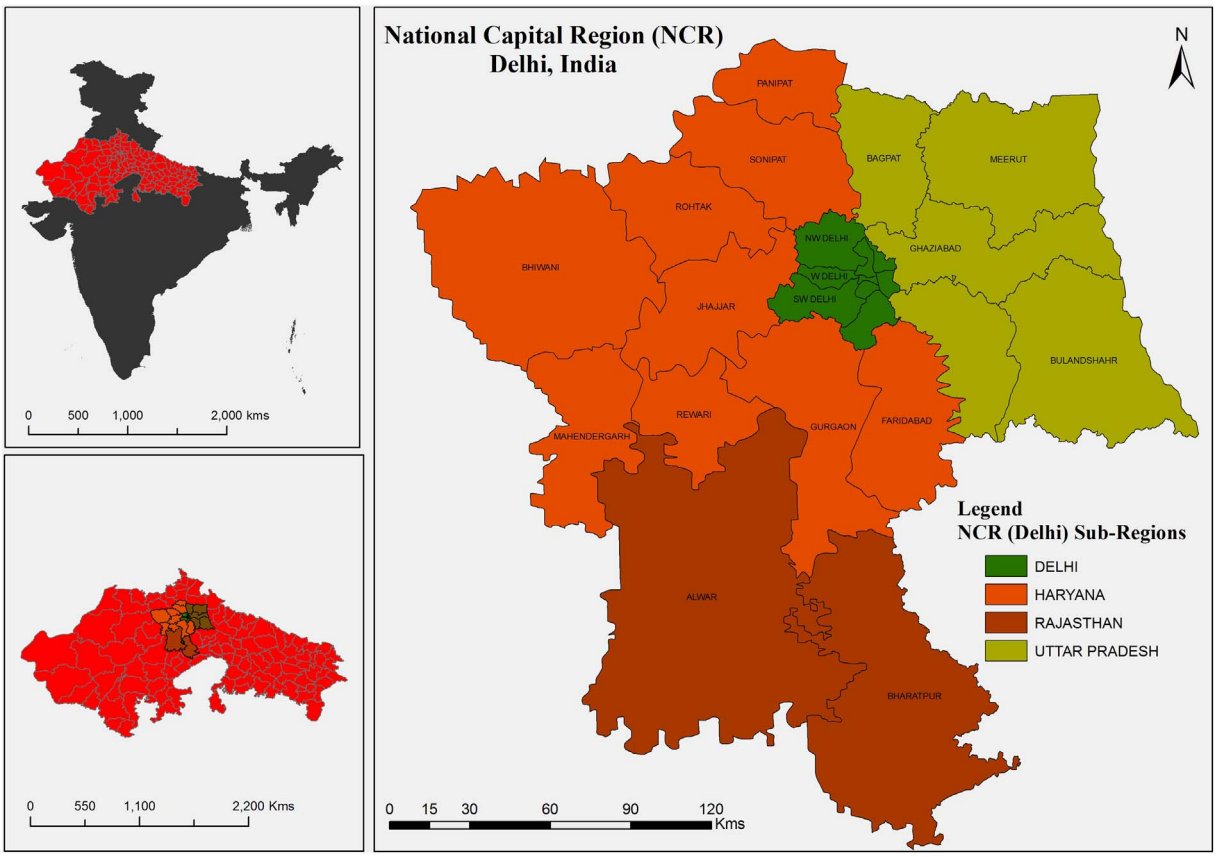

Fig. 1. Study area.

Table 1
Details of data used in this study.

Data acquired	Data acquisition date	Sources
Landsat 8 path/raw 146/40	2014-05-16	http://glovis.usgs.gov/
Landsat 8 path/raw 146/41	2014-05-16	http://glovis.usgs.gov/
Landsat 8 path/raw 147/40	2014-05-07	http://glovis.usgs.gov/
Landsat 8 path/raw 147/41	2014-05-07	http://glovis.usgs.gov/
Topographical maps 1:25,000	1996	SOI, India

8: the Operational Land Imager (OLI) and the Thermal Infrared Sensor (TIRS). OLI Sensor collects image for nine shortwave spectral bands with the swath distance and spatial resolution of 190 km and 30 m respectively for all bands except the panchromatic band. TIRS collects image data for two longwave spectral bands over a 190 km swath, with a 100 m spatial resolution. The shortwave spectral band 1 (with the central wavelength of 0.49 um) senses deep blues and violets. It is also known as the coastal/aerosol band, after its two crucial primary uses such as capturing the shallow water and tracking fine particles like dust and smoke. Bands 2, 3, and 4 are visible blue, green, and red. The near-infrared (NIR), band 5, of the spectrum is especially significant for ecology and environment purpose because healthy vegetations reflect it. Compare with other bands; we calculate the indexes like NDVI, which helps to measure vegetation health status more precisely than if we only looked at visible greenness. The shortwave infrared (SWIR) is captured by band 6, and 7 are particularly useful for depicting dry earth from wet earth, and for geology: rocks and soils that look similar in other bands often have strong contrasts in SWIR. Spectral band 8 is the panchromatic band (spectral; resoultion15 meters). It works just similar to black and white picture, instead of collecting visible spectrum separately; it combines them into one band or channel. Spectral band 9 shows the minimum significance, yet it is one of the most exciting features of Landsat 8. It covers a skinny slice of spectral wavelengths: (1370 ± 10 μm). Few satellite remote sensing based instruments collect this part of the spectrum because the atmosphere absorbs almost all of it. Landsat 8 turns this into an advantage. Precisely as the ground is barely visible in this band, reflecting very brightly. Here it is picking up fluffy cumulus clouds, but it is designed primarily for cirrus clouds. The thermal infrared or TIR captures band 10 and 11. Instead of measuring the atmospheric temperature, as weather stations do, they report on the ground itself, which is often much hotter than the air. There is significant uncertainty in the band11 values; it is recommended to

use TIRS band 10 data in a quantitative analysis of the TIRS data. It also suggests that band 10 be used in conjunction with an atmospheric model to estimate surface brightness temperature. Hence, band11 has not been used for environmental and energy budget studies as the other bands have. Table 1 shows the details of data used for the present study.

The commonly used GIS, DIP and statistical software, i.e. ERDAS, ENVI, FLAASH, ArcGIS, and SPSS software used for this study. The equipment TELATEMP Infrared Thermometer (Model AG-42 Telatemp Crop, Fullerton, CA, USA) used to measure the in-situ surface temperature.

2.3. Methodology

Satellite datasets of Landsat-8 level-1TP (Level 1TP product contains systematically, radiometrically, geometrically, and topographically corrected using GCPs) over NCR, India used for the preparation of LCLU map, NDVI, LSE and LST. DN (Digital number) data converted to at-sensor radiance for Landsat-8 data (https://landsat.usgs.gov/landsat-8-l8-data-users-handbook). ENVI-FLASSH (Fast Line-of-sight Atmospheric Analysis of Spectral Hypercubes) an atmospheric correction module used to retrieve spectral reflectance. Land surface temperature (LST) retrieves with the improved mono-window algorithm from the Landsat-8 Thermal Infrared Sensor Band 10 and the proportion of vegetation cover coupled with NDVI used for the estimation of ground emissivity of NCR, India. The mapping of land cover and land use, image classification performed to extract thematic information from the multispectral Landsat-8 image. The following sub-heading described the details of the methods adopted for this study.

2.3.1. Digital image classification technique

Digital image classification (DIC) techniques refer to the computer assisted interpretation of images, a process that is important to GIS (Lo and Yeung, 2007). The digital image classification techniques are to classify the pixels in an image into LCLU automatically. The supervised classification one of the approaches to digital image classification, significantly high accuracy level for LCLU mapping, however, it influences on the quality of the training sets (Nichol, 2005). Training sites are sample areas signifying each identifies LCLU category that seems relatively homogeneous on the image. This approach requires knowledge of ground truth on LCLU that obtained field work. The selection of training sites is a vital process because it affects the accuracy of the classified image. Therefore, the selection of pixel should be homogeneous values for each category of LCLU to be classified. However, in practical, it is difficult to have total homogeneity, and confusion between some LCLU categories will arise (Lo and Yeung, 2007). All the supervised classifications (viz. maximum likelihood and minimum distance classifier) usually have a sequence of processes (1) specifying the training sites, (2) obtaining the spectral signatures and (3) image classification. The training site being digitised, the next steps to create statistical characterizations of the data (mean vector and the covariance matrix of the spectral cluster) known as spectral signatures. Usually, five or six training sites are defined. The high accuracy can be achieved by selecting more training sets. This process verifies both the accuracy and correct interpretation of the image. After that, the classification of the image was carried out using Maximum likelihood classification (MLC) which is based on Bayesian probability theory. The MLC technique is preferred because it is the most robust classification technique when appropriate training sites defined (Jensen, 1996). Moreover, it is one of the widely used supervised classification techniques. MLC technique computes the probability that a pixel belongs to a particular class (more details could be found in Lo and Yeung, 2007).

In this study, the supervised classification carried out using the MLC technique with ERDAS Imagine software. LCLU classification scheme adopted based on the Anderson classification scheme (Anderson et al., 1976) as follows: built up, water body, sparse vegetation, dense vegetation, agriculture cropland, scrubland and fallow land, and bare soil and exposed rocks. One of the most critical procedures of image classification is accuracy assessment. The LCLU classes require validation with data collected from fieldwork. The classified image accuracy assessed by independent point data collected (i.e., GCPs) during the fieldwork, Google map, and derived LCLU maps. A total of 358 sample GCPs were selected using the random stratified method to assess the accuracy of LCLU map. The details about the accuracy assessment techniques discussed in Lillesand and Kiefer (1999). The overall accuracy of LCLU map was 89.21%, and Kappa coefficient was 0.877, which indicated the classified LCLU map could satisfy the future analysis requirement. The producer's accuracy in some of the classes viz., built-up (76.68%) and agricultural cropland (82.52%) classes etc. indicate significant confusion with other LCLU because it attributed to intermixing in the classes and, uncertainty in spectral reflectance in the particular features class. Some of the LCLU categories viz., water bodies, bare soil and exposed rocks depicted significantly higher accuracy.

2.3.2. Conversion of DNs to physical units

At-sensor radiances measured at a wavelength spectrum which captures the image in Digital Numbers (DNs). DN values have no unit and any physical implication; therefore, it is essential to coverts to radiance then to at-sensor (top of atmosphere) brightness temperature and, after that, to land surface temperature (LST) using the improved mono-window algorithm, thereby it assists for quantitative analysis of thermal remote sensing data.

2.3.3. OLI and TIRS at sensor spectral radiance

Satellite images are processed in units of absolute radiance using 32-bit floating-point calculations. After that, these values were converted to 16-bit integer values. It can then be converted to spectral radiance using the radiance scaling factors provided in the metadata file of Landsat-8:

$$L_\lambda = M_L{}^{*}Q_{cal} + A_L \quad (1)$$

where:

L_λ = Spectral radiance ($Wm^{-2}sr^{-1}\mu m^{-1}$).

M_L = Radiance multiplicative factor for the band (RADIANCE_MULT_BAND_n from the metadata).

A_L = Radiance additive factor for the band (RADIANCE_ADD_BAND_n from the metadata).

Q_{cal} = Pixel value in DN.

2.3.4. Atmospheric correction

ENVI-FLASSH (Fast Line-of-sight Atmospheric Analysis of Spectral Hypercubes) an atmospheric correction module used to retrieve spectral reflectance. The standard atmospheric (tropical atmosphere) and the geometric parameters (such as aerosol, CO_2, azimuth, zenith angle, square slit, etc.) calculated using the FLAASH module (Detail could be found in the weblink). The atmospheric parameters (such as water vapour and Aerosol Optical Depth (AOD)) procured from the AERONET (AErosol RObotic NETwork) and incorporated into the FLAASH module.

2.3.5. Estimation of ground emissivity using empirical method

Natural surfaces of NCR, India are heterogeneous at the pixel level in respect to emissivity variation. The observed ground emissivity value shows land-cover and strong seasonality dependence. Primarily, it depends on soil moisture, land-cover, soil organic composition, vegetation density, and structure. Such as densely vegetated areas the broadband (ε_{8-14}) emissivity is usually found in-between 0.96 and 0.98, and for the bare soil 0.90 or less (Jin and Liang, 2006). In this study, an effort was made to derive ground emissivity by opting the proportion of vegetation cover coupled with NDVI using Landsat-8 satellite data. The proportion of vegetation cover is estimated using the Eq. (2) (Valor and Caselles, 1996; Mallick et al., 2008):

$$P_V = \frac{\left(1 - {}^{NDVI}/_{NDVI_g}\right)}{\left(1 - {}^{NDVI}/_{NDVI_g}\right) - k\left(1 - {}^{NDVI}/_{NDVI_v}\right)} \tag{2}$$

where,

$NDVI_g$ = NDVI value of pure soil pixel.

$NDVI_v$ = NDVI value of pure vegetation pixel

$$k = (\rho_{NIRv} - \rho_{REDv})/(\rho_{NIRg} - \rho_{REDg})$$

where ρ_{NIRv} ρ_{REDv} are reflectance in the near infrared (band5) and red (band4) region for pure vegetation pixels; ρ_{NIRg} and ρ_{REDg} are the reflectance in the near infrared (band5) and red (band4) region for pure soil pixels respectively. Herein, the model has two steps. The first step, the vegetation and bare soil proportions obtain from the NDVI of pure pixels, and a second step proportion of vegetation cover coupled with Normalized Difference Vegetation Index (NDVI) used for deriving the ground emissivity.

The estimation of NDVI of mixed pixels (i.e. mixture of bare soil and vegetation) is estimated using Eq. (3)

$$NDVI = NDVI_v P_v + NDVI_s(1 - P_v) + di \tag{3}$$

where $NDVI_v$ is the pure pixel of vegetation NDVI $NDVI_s$ is the pure pixel of soil NDVI in the studied area, and di is the error in NDVI. The emissivity and error in emissivity was calculated using Eq. (4)

$$\varepsilon_{(8-14)} = \frac{\varepsilon_v - \varepsilon_s}{NDVI_v - NDVI_s} NDVI + \frac{\varepsilon_s(NDVI_v + di) - \varepsilon_v(NDVI_s + di)}{NDVI_v - NDVI_s} + d\varepsilon \tag{4}$$

where $d\varepsilon$ is calculated from Eq. (5)

$$d\varepsilon = (1 - \varepsilon_s)\varepsilon_v F(1 - P_v) + [(1 - \varepsilon_v)\varepsilon_s G + (1 - \varepsilon_v)\varepsilon_v F'] P_s$$

Alternatively, in a simplified form:

$$d\varepsilon = 4(d\varepsilon)P_v(1 - P_v) \tag{5}$$

where P_v is the proportion vegetation cover; P_s is the fraction cover of soil; ε_v is the vegetation emissivity; ε_s is the emissivity of the bare soil. F refers shape factors that take into the account the fraction of radiation that reaches the ground coming from the vegetation side, G the proportion that reaches the side coming from the ground, and F' the fraction that effects from the surrounding (Caselles and Sobrino, 1989). The estimation of error in emissivity value ($d\varepsilon$) is the average weighted value that accounted the emissivity value of different surface types. Therefore, the weighted value ($d\varepsilon$) of 0.04 opted in this study area. For the ground emissivity values estimated the term ε_v and ε_s, i.e., the emissivity values of pure vegetation pixel and pure soil pixel, are taken as 0.978 and 0.914, respectively from published literature value (Valor and Caselles, 1996; Mallick et al., 2008).

Many published research works (Sutherland (1986); Labed and Stoll (1991); Elvidge and Chen (1995) show the vegetation depicted in near-grey body behaviour in the whole 8–14 μm spectral wavebands. Therefore preassumed that the ground emissivity in narrow-bands will equal (approx.) to the emissivity corresponding to the 8–14 μm spectral wavebands. On the other hand, the exposed rock materials and soils have spectra with differing characteristics that do not follow grey-body behaviour (Sutherland, 1986; Labed and Stoll, 1991; Salisbury and Daria, 1992). Rubio et al. (1997) proposed the equation which shows the good correlation between broadband and narrow-band emissivity. Hence, correlation equation is used to derive the effective emissivity as below mentioned.

Table 2
Gain (x) and Intercept (y) value to derived ground emissivity for narrow-bands of Landsat-8.

	a	b	σ
Vegetation	–	–	–
ε_{10}	1.549	- 0.539	± 0.007
Soils	–	–	–
ε_{10}	0.101	0.877	± 0.006

$$\varepsilon_i = x^*\varepsilon_{8-14} + y \tag{6}$$

where ε_i is band 10 of Landsat 8, Table 2 shows the value of gain x and intercept y.

2.3.6. Estimation of surface temperature using mono-window algorithm

Band 10 of Landsat 8 imagery converted from spectral radiance (as discussed in Section 2.3.3) to a more physically valuable variable (https://landsat.usgs.gov/landsat-8-l8-data-users-handbook-section-5). The effective temperature based on remote sensing sensor viewed Earth-atmosphere system under an assumption of fixed ground emissivity and using pre-launch calibration constants (Schott and Volchok, 1985). The digital numbers (DNs) of the thermal infrared band (TIR) is converted into spectral radiance (L_λ) using the calibration constants, and incorporation of ground emissivity estimates the LST. In case of non-availability of radio-sounding in the Radiative Transfer Equation (RTE) method, Qin et al. (2001) developed the following mono-window algorithm for obtaining LST using Eq. (7):

$$T_s = \frac{1}{C}^*\left[X^*(1 - C - D) + Y^*(1 - C - D) + (C + D)*T_{sensor} - DT_a\right. \tag{7}$$

with,

$$C = \varepsilon\tau,\ D = (1 - \tau)*[1 + (1 - \varepsilon)\tau]$$

X = −67.355351, Y = 0.458606, and

where ε is the land surface emissivity, τ is the total atmospheric transmissivity, T_{sensor} is the at-sensor brightness temperature, and T_a represents the average atmospheric temperature given by Eq. (8):

$$T_a = 16.0110 + 0.92621^*T_0\ (Mid - latitude\ summer) \tag{8}$$

T_0: the near surface temperature, Qin et al. (2001) also estimate the atmospheric transmissivity from *w*, the atmospheric water vapour content, for the range 0.4–1.6 g/cm^2.

2.3.7. Result validation

Ground-truthing data collections are essential to verify the estimated ground emissivity from Landsat-8. In the present study field measurements (in situ) emissivity value as well as the published literature values were compared with estimated ground emissivity.

2.3.7.1. Field measurements of emissivity. The emissivity box has been used for field-based (in-situ) measurements of ground emissivity (Kant and Badarinath, 2002; Mallick et al., 2008; Mallick et al., 2012). The handheld Infrared radiometer (TELATEMP: AG-12) used to measure the temperature, which operates in the 8–14 μm spectral wavebands with an Instantaneous Field of View (IFOV) of 2° with an accuracy of 0.1 °C. The field observation or measurement was done at predefined locations of NCR, considering different surface materials on all clear sky (no cloud) at different hours (10.00 am to 11.30 am) of the day.

The ground emissivity values are the results of field-observed measurements in and around NCR area. The measurements restricted to selected (dominant) ground features representing different LCLU classes. The ground measurements performed on bare soil, dense vegetation, grass, agricultural paddy crop and urban surfaces (concrete). The emissivity measurement carried out when the observation gets stabilised. The value of the ground emissivity measured for vegetation (leaves) and soil samples (with the average 4–5 values of the respective samples) by the emissivity box method using the infrared radiometer. The measured emissivity value is shown in Table 3. The average determined as a final emissivity value of the observed materials that used in practice whereas the variability in emissivity values shown as standard deviations. It inferred from the Table 3 that there is a little variation in the ground-based measured emissivity values.

The retrieved emissivity value also (Table 3) compared with those measured by different researchers such as Owe and Griend, 1994 was carried out in the tropical area of the loamy sand type in 8–14 μm spectral wavelength (ε = 0.914) and Mallick et al., 2008 in a semi-arid region of Delhi. The obtained value has satisfactory results compare with the measured field values. The satellite-derived emissivity over soil (ε = 0.9212), open grass (partly covered) (ε = 0.949) and over grass in parks (ε = 0.9541) is shown in Table 3. The derived ground emissivity values over different features have also been compared with those values available in the literature and found to be in good agreement (error of around 1–2%).

Table 3
Emissivity value measured during field campaign for different samples.
Sources: Abbreviations in 'Source' column stand for: BK Buettner and Kern (1965), CZ Chen and Zhang (1989), HM Husband and Monteith (1986), J Jin (1990), LS Labed and Stoll (1991), OG Owe and Griend (1994), S Sutherland (1986), VC Valor and Caselles (1996), VDI Verein Deutscher Ingenieure (1992), WHM Wang et al. (1994), MJ Mallick et al. (2008).

Features	Mean	Satellite derived emissivity	UTM coordinates WGS 84	Derived emissivity values from literature
Dense vegetation	0.9695 ± 0.07	0.978	77°11′21.557″E 28°33′2.199″N	MJ (0.9745)
Grass	0.9610 ± 0.010	0.971	77°15′10.063″E 28°36′11.261″N	LS (0.979–0.983), S (0.966–0.990), J (0.983), MJ (0.954), WT (0.982)
Agricultural paddy cropland	0.9742 ± 0.014	0.976	77°1′56.332″E 28°50′59.78″N	MJ (0.972)
Urban surface (concrete)	0.9182 ± 0.011	0.902	77°10′47.231″E 28°40′40.369″N	VDI (0.92–0.95), BK (0.966), J (0.914), MJ (0.918), WT (0.937)
Bare soil	0.9172 ± 0.011	0.913	76°57′34.747″E 28°33′17.518″N	VDI (0.92 = farm soil, 0.86–0.92 = sand) BK (0.914–0.936), S (0.893–0.958), OG (0.914–0.957), VC (0.948–0.952), J (0.907–0.969), MJ (0.921),

2.4. Comparison of observed (in-situ) and estimated surface temperature

The satellite and ground-based measured LST analysed for the comparison. The comparison of satellite-derived LST with that of ground measured values conducted over the same coordinate locations (GPS) using TELETEMP infrared thermometer which operates in the 8–14 lm wavelength with an instantaneous field of view (IFOV) of 2° with an accuracy of 0.1 °C and a field of view of a 4° cone. To minimise any influence of the exposed soil, the instrument held to view the surface material at an angle of 55–60° from the nadir. It captured at a typical distance of 1–3 m depending on feature materials accessibility (Table 4). The field observation was done at predefined locations of NCR, considering different surface materials on all clear sky (no cloud) at different hours (10.00 am to 11.30 am) of the day. The dense vegetation (tree cover), grass (park), agricultural paddy cropland and bare soil and built-up materials which were more dominant in the study area considered for the in-situ measurement. It observed that the estimated LST values from Landsat-8 satellite imagery are in close agreement with that of ground measured data within an error of 1.5–3 °C (compared to the same solar time of satellite pass). The correlation coefficient between the satellite-derived and field observed surface temperature is very high $R = 0.927$ (correlation-coefficient significant at the 0.01 level). Therefore, it concluded that the comparison between the satellite-based retrieved temperature and field observed found in good agreement (Caselles et al., 1997; Weng and Quattrochi, 2006; Mallick et al., 2008; Mallick et al., 2012).

Table 4
Comparison of retrieved LST with field measurement data.

Features	[a]Field observation during 10 to 12 May 2014 (10.00 to 11.30 local time) in degree Celsius	Satellite observation LST in degree Celsius	UTM Coordinates WGS 84
		LANDSAT 8 25th May 2014	
Dense vegetation 1 (*Prosopis juliflora*, Bougainvillea in forest)	27.70	29.25	77°11′21.557″E 28°33′2.199″N
Dense vegetation 2 (*Prosopis juliflora*, Bougainvillea in forest)	27.90	28.40	77°9′46.324″E 28°36′48.697”N
Grass (open space) (Azadirachtaindica A. Jurr)	31.1	33.60	77°15′10.063″E 28°36′11.261”N
Grass (open space) (Azadirachtaindica A. Jurr)	34.7	36.47	77°12′10.747″E 28°35′4.282”N
Concrete (dense built-up)1	34.10	36.52	77°10′47.231″E 28°40′40.369”N
Concrete (dense built-up)2	34.90	37.36	77°13′5.464″E 28°39′27.941”N
Road side build up area	38.20	40.68	77°19′35.548″E 28°37′5.966”N
Industrial area 1	42.9	44.91	77°9′37.674″E 28°41′49.643”N
Industrial area 2	40.8	43.60	77°16′33.943″E 28°32′12.42”N
Bare soil	40.50	43.01	76°57′34.747″E 28°33′17.518”N

[a] Average values of at least 4–5 measured samples.

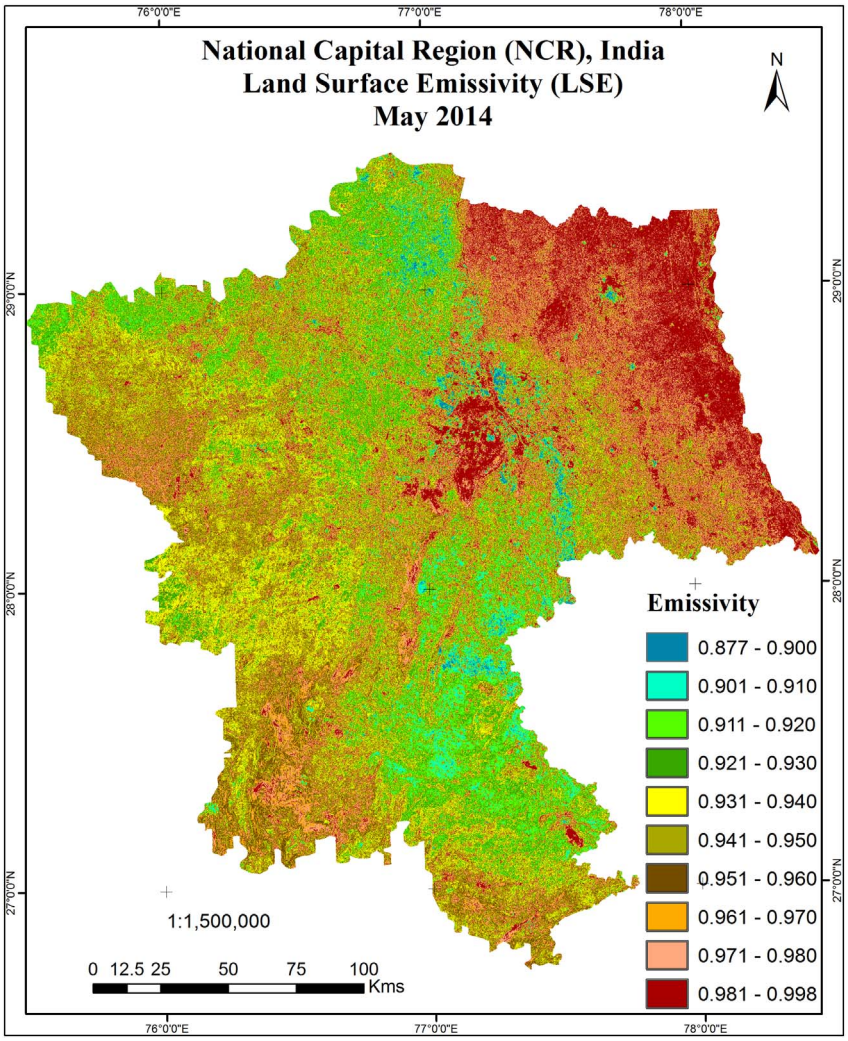

Fig. 2. Geospatial distribution of surface emissivity estimated from LANDSAT 8 data. (For interpretation of the references to colour in this figure, the reader is referred to the web version of this article.)

3. Results and discussion

3.1. Assessment of satellite-derived emissivity

The availability of ground-based emissivity measurements using the box method (Sobrino et al., 1993; Mallick et al., 2008) allows us to experiment with the results obtained by empirical method (proportion of vegetation cover coupled with NDVI). For this purpose, Eq. (6) applied to the satellite image of LANDSAT-8 and the ground emissivity values obtained for those plots where the ground-based emissivity measurements performed.

Fig. 2 shows the geospatial distribution of ground emissivity estimated from LANDSAT-8 data. The ground emissivity values lie between the range of 0.877 to 0.998, with a mean value of 0.923 and standard deviation (Std. Deviation) of 0.0198. The high emissivity values, ranging from 0.961 to 0.998 depicted in orange to dark brown colour. It observed in the central ridge area, eastern, northeastern, west, south and southwest part of the study area corresponding to agricultural land, sparse vegetation (10% to 40% canopy cover area) and dense vegetation (> 40% canopy cover). The moderate emissivity values range between 0.921 and 0.960 shown in dark green to dark greenish. These values noticed in the west, northwest and southern part of the study area which is corresponding to sparse vegetation and scrubs land. The low emissivity values ranging from 0.877 to 0.920 (sky blue to green areas) observed over built-up areas and bare soil. It geographically situated in the south-central, north, northwestern and central part of the study area. This area the ground emissivity is lower due to spectral emissivity that depends upon the types of surface materials, for example, built-up structures have more reflectance and lower absorption rate (lower emissivity) than the green vegetated cover (higher emissivity).

The Fig. 3a and b represent the ground emissivity variation for different landscape classes and its corresponding histogram. The

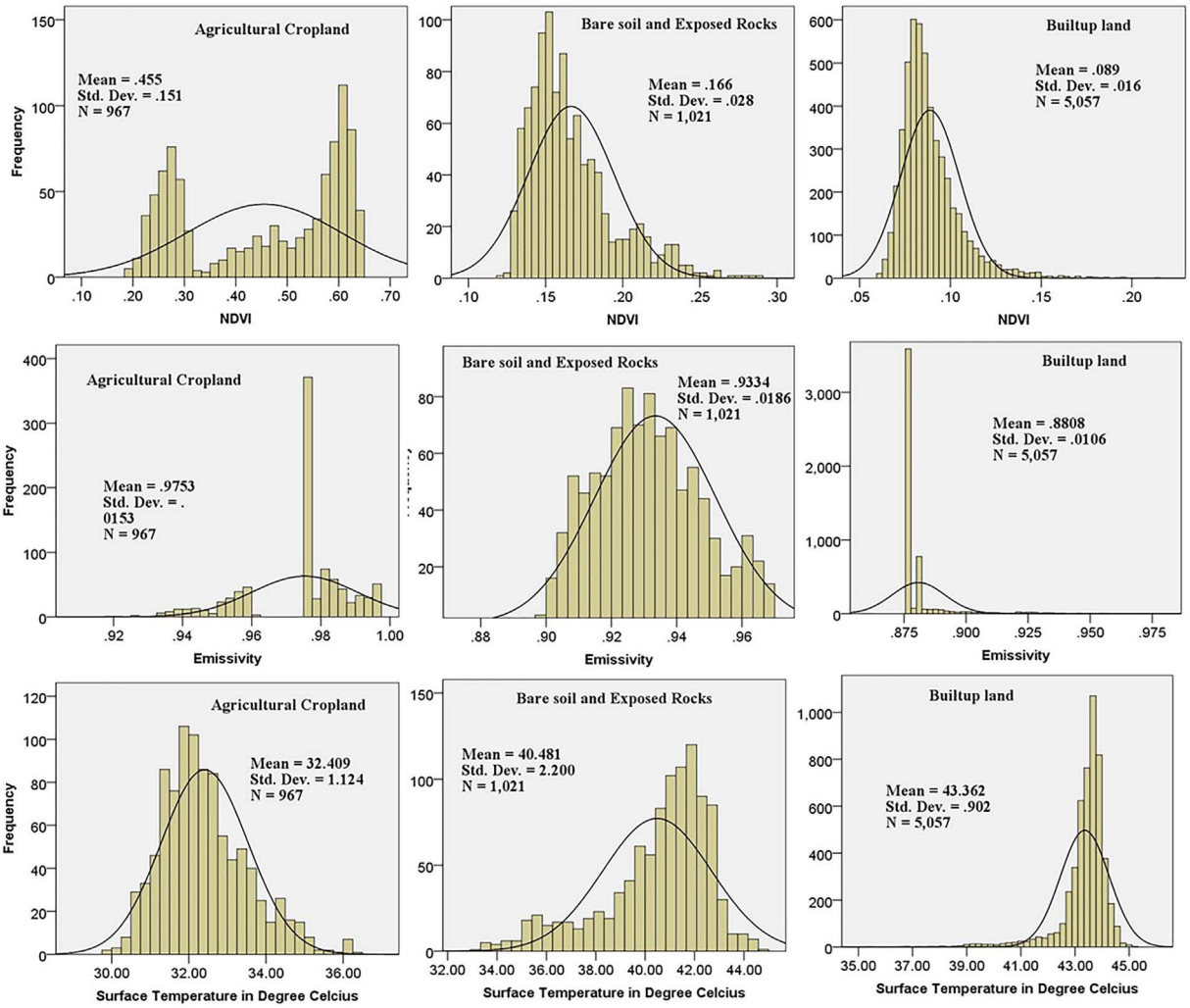

Fig. 3. a: NDVI, Emissivity and LST over the different LCLU and its related histogram.
b: NDVI, Emissivity and LST over the different LCLU and its related histogram.

maximum ground emissivity values observed over agricultural cropland (Fig. 3a) that ranges between 0.921 and 0.991 (mean 0.975 and Std. Deviation 0.0153). The peak spikes percentage (histogram) of agricultural cropland at 0.971 to 0.985 which corresponds to the agricultural products such as pulses, sugarcane, and wheat grow in this agricultural area of the region with small patches of horticulture (mainly seasonal vegetables). The Pulses, sugarcane during May month was in the growing stage. Hence, most of the field had full extent with a minimum of the soil background. As a result higher ground emissivity value. The std. deviation value of emissivity was significantly lower for pulses and sugarcane crop (agricultural cropland) owing to their homogeneity.

The built-up class value is ranging from 0.877 to 0.9393 with a mean value 0.8808 and Std. Deviation 0.0106. The peak percentage (Histogram) of the built-up is at 0.877–0.900 about 80%. Significant variations, ranging from 0.897 to 0.967 observed for bare soil with a mean value 0.9334 and standard deviation 0.0186 (Fig. 3b), with a peak of about 44% at 0.920 to 0.944. This substantial variation is partly due to the underlying soil characteristics and the growing state of the agricultural fallow land.

The emissivity results comparison shows that the range of ground emissivity for dense vegetation (Fig. 3b) is much more moderate than that of built-up and bare soil, with the maximum emissivity of 0.975 and the lower limit as on 0.995. The histogram (Fig. 3b) has evident peaks at 0.98 and 0.99 above 70% and small percentage at other emissivity values. The higher and lower emissivity values noticed, but rarely, and are considered to be mixing with other surface types. The range of emissivity for scrubland (Fig. 4b) varies from 0.895 to 0.9776 (mean 0.9598 and standard deviation 0.0268). Significant variations, ranging from 0.897 to 0.996 are observed for sparse vegetation with a mean value 0.977 and standard deviation 0.0184 (Fig. 3b), with a peak of about 90% at 0.94 to 0.992. These large variations are partly due to the underlying soil conditions and partly due to the growing state of the agricultural fallow land. There is significant variation in the emissivity values in the sparse vegetation type due to the emissivity value of the bared soils is highly variable.

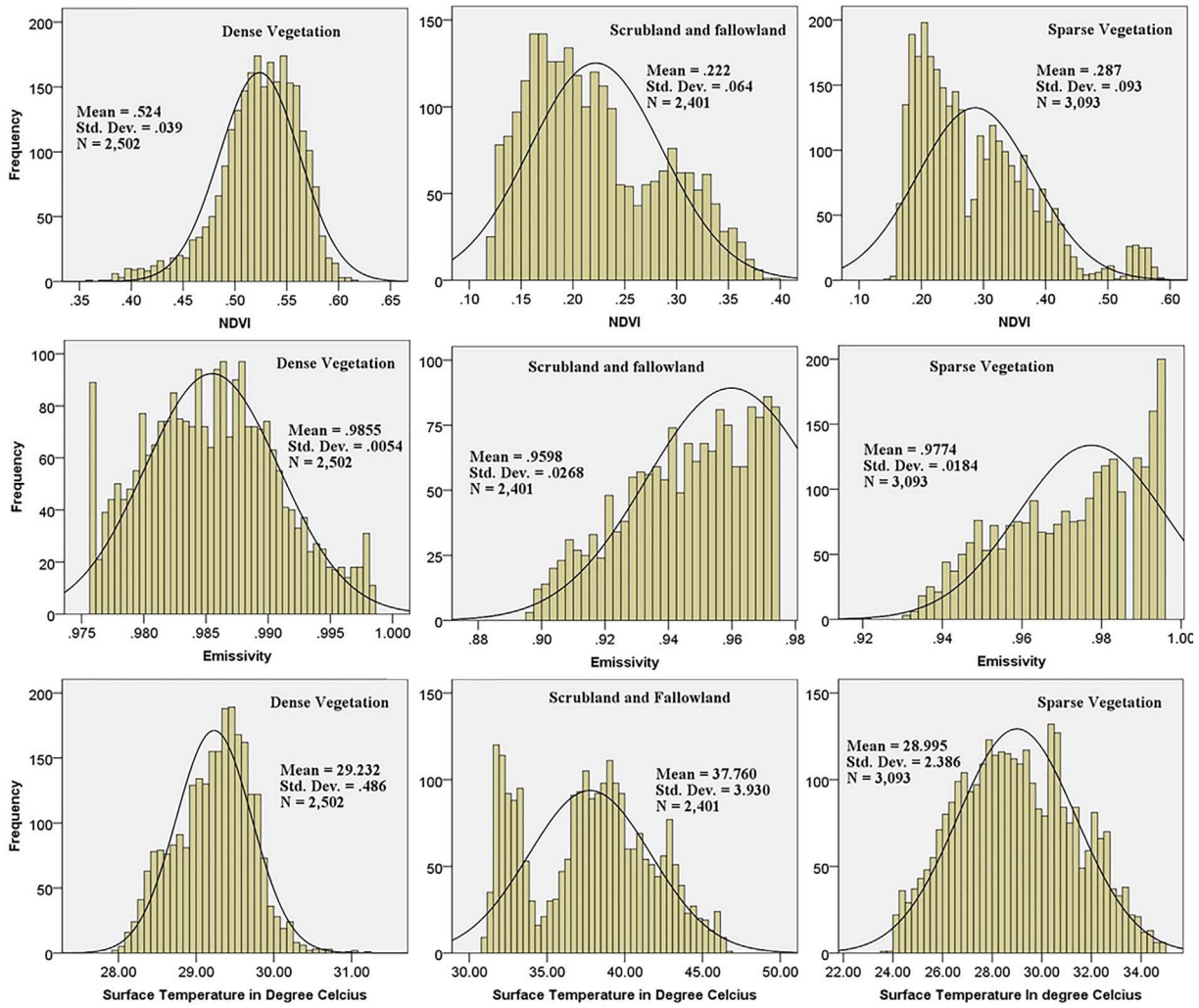

Fig. 3. (*continued*)

3.2. Analysis of land surface temperature derived from LANDSAT-8

The spatial distribution of LST retrieves with the improved mono-window algorithm from the Landsat-8 Thermal Infrared Sensor Band 10 is shown in Fig. 4. The LST is ranging between from 24.63 °C to 54.19 °C with a mean of 40.09 °C and Std. Dev. of 4.48. It noticed from the derived map that west and southwest part of NCR exhibits the highest surface temperature (40 to 46 °C) mainly due to the agricultural fallow land, scarcity of vegetation. Some hotspots are observed over the bare soil distributing in the suburban area. Some of the high-temperature zones are also seen in the central and southeastern part of the map mainly due to commercial/industrial land use which often contains much bare land, reflective materials with low emissivity and the impervious surface are also higher than that of the high dense built-up area due to industrial fumes. Towards the south and western part of the study area exhibits higher temperature (43 to 54 °C) due to built-up land, bare soils, and scrubland/fallow land use. It is also noticed from the derived map that same significant temperature pattern over the city area, which was located in the highly dense built-up area and scarce of vegetation. The moderate level of surface temperature (37 to 43 °C) observed in the north, patches in the east and southwest part of NCR regions which distributed over the sparse and scrubland.

It notices that the north, east, central ridge area exhibits the lower surface temperatures (24 to 37 °C) due to the agricultural cropland and dense vegetation. Marshy land and water bodies exhibit the lowest surface temperature (24 to 38 °C). In the city centre area (NCT, Delhi) such as Cannought place, Chandni Chowk and its surrounding densely populated areas show the significant thermal effects, which could be visually characterized by the spatial pattern phenomena, extent, heterogeneity, and its higher intensity of impervious cover. The analysis of spatial distribution of LST over various land use types within the urban areas depicted that the high densities of imperviousness (concrete structures), less porous concrete materials and frequent commercial-industrial activities contribute to the change in micro-climate over NCR (Yogesh et al., 2009).

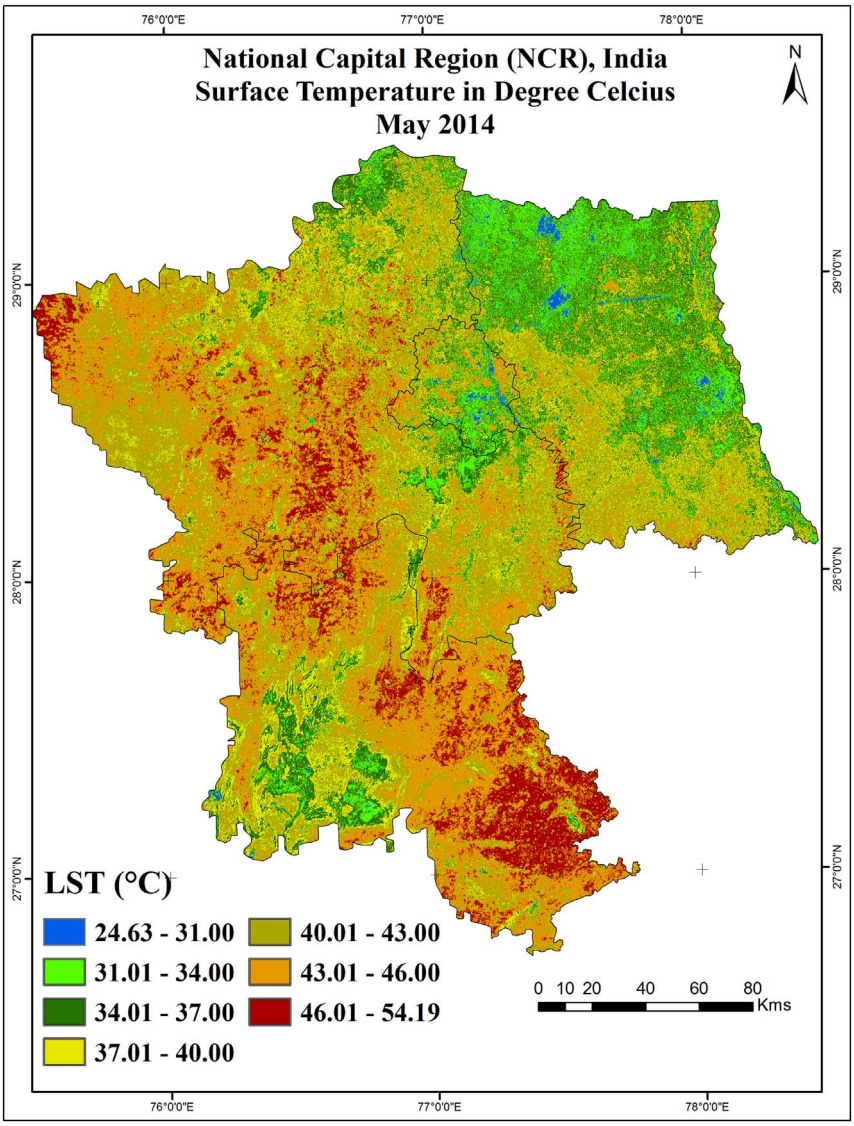

Fig. 4. Retrieved LST Maps from Landsat-8 data.

3.3. Effects of LST over land cover/land use

For the geoscientific assessment of surface temperature over the landscape characteristics, the land cover/land use map has been developed using supervised classification techniques using digital image processing software (maximum likelihood classifier: MLC). Fig. 5 shows LCLU of NCR of 2014 that shows the built-up area (red colour) is mainly located in the southeastern and southwestern and central part of the NCT, Delhi, whereas in Uttar Pradesh, it populated mainly in the western part at the bank of Yamuna River.

The statistics of land cover/land use classes depicted in Table 5, and it found that the most dominant class is the scrubland and fallow land occupies 71.20% of the total area of NCR, India. The area under vegetation cover (sparse and dense vegetation) accounted about 14.11%. Whereas, the built-up area which impervious cover and has an environmental concern because of their low-grade concrete materials (lower emissivity), poor planning leads to the highly dense build up area geographically spread approx. 2.64% of total area of NCR.

The accuracy assessment performed for the derived LCLU map. It noticed that the overall accuracy of the map is 88.42% with the kappa statistics of 0.8646. The accuracy level of the feature class also calculated and it noticed that the highest user accuracy found in water bodies (96.01%). Followed by agricultural land (92.48%), whereas the low user-accuracy identified in dense vegetation area (82.92%) due to the mixing of spectral reflectance of pixels with agricultural cropland feature class.

The retrieved LST values over different land cover/land use classes as shown in Table 6. In Rajasthan, NCR the maximum surface temperature noticed over bare soil range between from 41.21 °C to 48.14 °C with a mean of 46.39 °C and Std. Dev 1.29. Whereas in NCT, Delhi the maximum surface temperature found over the impervious built-up lands range between from 36.21 to 46.11 °C with a

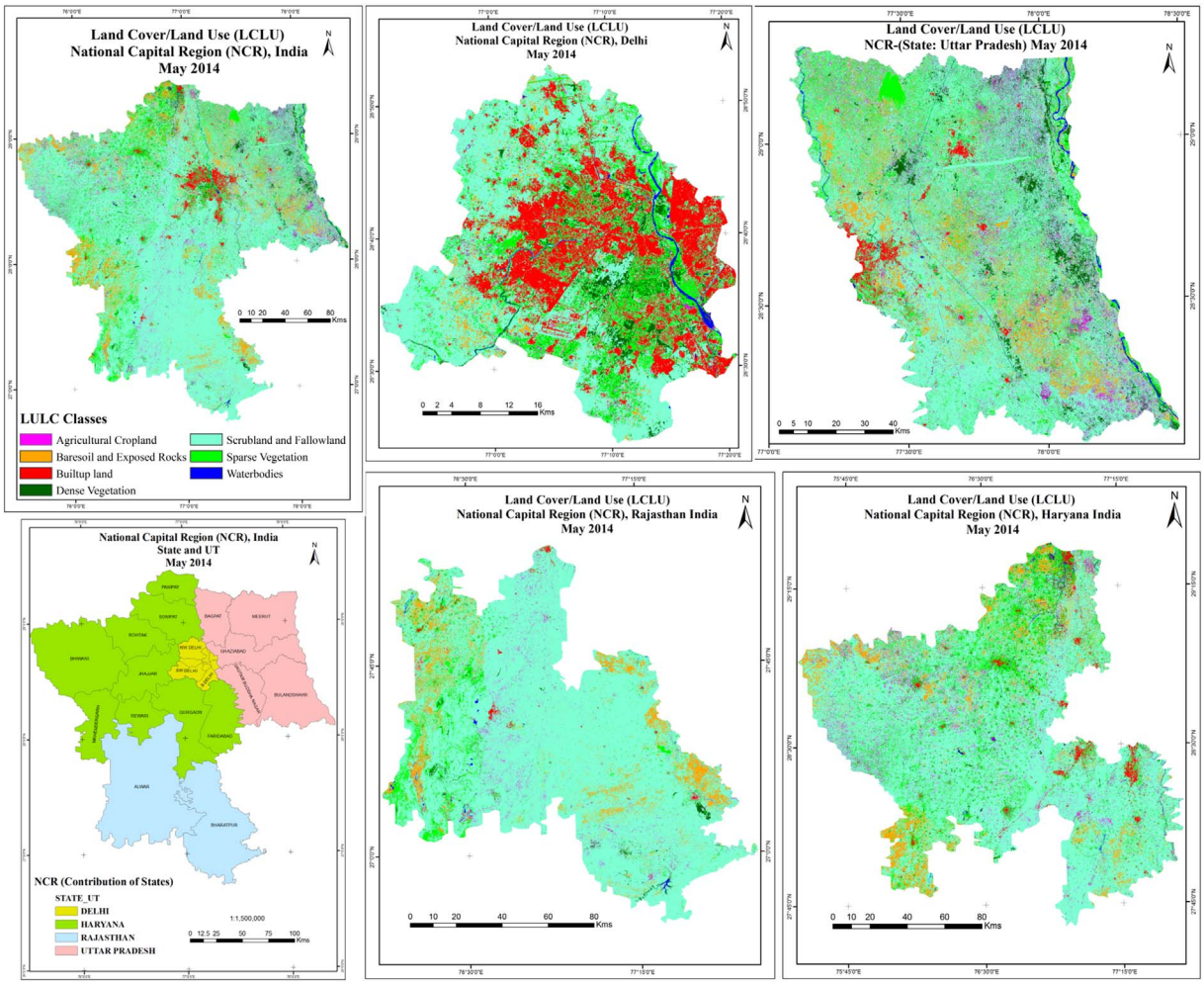

Fig. 5. LCLU map of NCR, India. (For interpretation of the references to colour in this figure, the reader is referred to the web version of this article.)

Table 5
LCLU map of NCR, India (2014).

Sl.No	Land use/land cover	Area in Sq. km	Percentage %
1	Water bodies	289.54	0.63
2	Sparse vegetation	5704.81	12.47
3	Scrubland and fallow land	32,568.15	71.20
4	Dense vegetation	749.97	1.64
5	Built-up land	1207.03	2.64
6	Bare soil and exposed rocks	3279.14	7.17
7	Agricultural cropland	1940.34	4.24
Total		45,740.00	100.00

mean of 45.24 °C and Std. Dev 1.29 this is due to highly populated built-up area, a chain of constructions events initiated that alters the urban air and water resources. Water has a high specific heat tended to get warm slowly during the daytime owing to its high thermal inertia, and to convection and turbulence (e.g., wave action). The distinctive characteristics of rivers, canals, and ponds concerning its physical and chemical properties tend to variation in their surface temperature values, leading to a high standard deviation value of 3.12 (NCT, Delhi) over water bodies. The average surface temperature of water bodies in NCT, Delhi and NCR, UP is 34.17 °C and 26.85 °C respectively.

The spatial trend of variation of surface temperature plotted on each class shows in Fig. 6. In NCT, Delhi, the built-up land has recorded the high surface temperature. The impact of vegetation notified as lower temperatures over agricultural cropland, dense vegetation (forest), sparse vegetation (grass/park). The different variety of vegetation types and its canopy level showed a significantly lower surface temperature as its properties to reduce the amount of heat stored in the soil and surface structures through

Table 6
LST in degree Celsius over the different LCLU, 2014.

NCR State/UT	Variable	Water bodies	Sparse Vegetation	Dense vegetation	Scrub land	Built-up	Bare soil	Agricultural cropland
Delhi	Min	26.30	28.48	26.60	27.84	36.21	37.10	30.37
	Max	36.80	45.73	30.48	45.33	46.11	44.52	36.01
	Mean	34.17	32.95	29.24	35.79	45.24	42.03	33.75
	STD	3.12	1.98	0.61	1.62	1.20	1.57	1.88
Haryana	Min	25.89	28.77	29.24	29.19	38.60	34.89	29.02
	Max	38.24	34.50	34.26	44.80	45.51	47.19	37.54
	Mean	30.83	31.45	31.42	38.03	44.00	42.71	32.52
	STD	3.74	1.28	1.07	1.29	1.49	1.27	1.37
Rajasthan	Min	23.77	30.03	27.50	30.43	34.62	41.21	27.44
	Max	42.81	41.53	44.77	46.54	45.59	48.14	42.33
	Mean	31.06	37.86	34.23	41.55	40.17	46.39	33.07
	STD	4.63	1.76	1.55	1.79	2.19	1.29	3.15
Uttar Pradesh	Min	25.81	21.30	27.93	33.40	37.59	33.39	29.48
	Max	38.05	37.13	34.08	45.92	46.42	51.39	36.41
	Mean	26.85	30.58	29.32	40.83	43.49	41.75	32.27
	STD	1.62	1.59	1.58	1.95	1.06	5.12	1.22

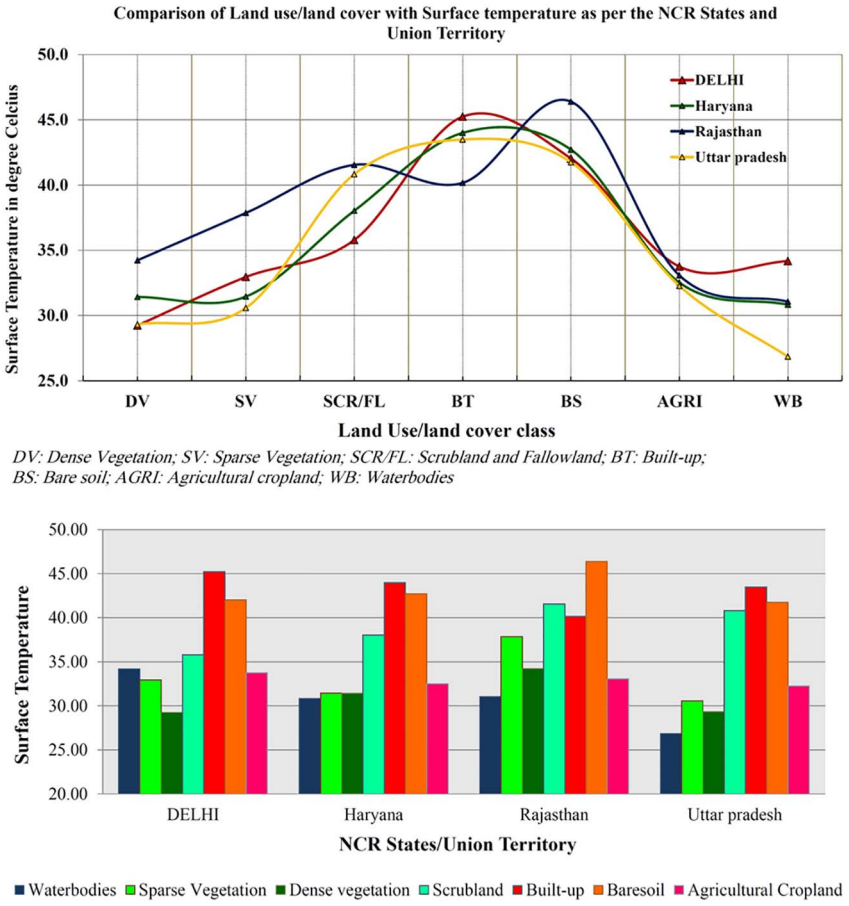

Fig. 6. LST over different LCLU.

evapotranspiration.

The spatial distribution of surface temperature in the densely populated urban area indicates the over LCLU feature class the high densities of the built-up surface, and low vegetation cover may contribute to the adverse change in micro-climate of NCR, India. Hence, the land characterization of regional thermal environment which is valuable parameters for urban planning and decision making.

The retrieved surface temperature values compared with the ground-based measurements which were held during a field campaign from 10 to 12 May 2014. The ground measurements performed over the bare soil, dense vegetation, grass, agricultural paddy

Table 7
Correlation between NDVI with LST.

Vegetation cover	NDVI	Surface temperature	Pixel count
NDVI	1.000	−0.843[a]	14,090
Land Surface Temperature	−0.843[a]	1.000	14,090

[a] Correlation is significant at the 0.01 level (1-tailed).

crop and urban surfaces (concrete) covering the land cover/land use types. As per the comparison and results analyse with the retrieved LST and ground-based temperature measurement confirm the acceptable range with an error of 2–3 °C (Kant and Badarinath, 2002; Mallick et al., 2008 and Mallick et al., 2012).

3.4. Response of vegetation density (NDVI) to surface temperature

Pearson's correlation between vegetation density (NDVI)-surface temperature was analysed of May 2014 (summer season) using SPSS (version 22.0), two-tailed *P*-values were taken to determine the significance. The total 14,090 counts (pixel) randomly selected to verify the relationship. NDVI correlated negatively with surface temperature (Pearson's correlation of −0.843) with the significant level of 0.01 (2-tailed) (Table 7). The areas are having low NDVI values show the high surface temperature. Linear regression coefficient computed, which assures prospective to simulated surface temperatures (summer season) if NDVI values are known (Fig. 8). The linear regression coefficient (surface temperature with NDVI) for different land cover/land use categories shown in Table 8. The cooling effects of vegetation density on surface temperature are much stronger during summer season (May 2014) thus the surface temperature related drought indices might only be valid for the summer season. This negative correlation due less rainfall occurred in the May months and might be due to the absence or limited vegetation cover (Fig. 7).

The most substantial regression coefficient between LST and NDVI values found over scrubland and agricultural fallow land ($R^2 = 0.704$) tailed by agricultural cropland ($R^2 = 0.704$) sparse vegetation ($R^2 = 0.679$). The strong correlation between surface temperatures with NDVI also observed over the scrubland, sparse vegetation and agricultural cropland, which may use a potential of using linear regression to simulate the surface temperatures of summer season if the NDVI values are known. Hence the result infers that during summer season or less rainfall area the surface temperature may be simulated with reasonable accuracy using NDVI value.

3.5. Implications of Geoinformation technology for regional planning and managing the thermal environment

An investigation of the relationship between satellite-retrieved land surface temperatures, the ground-based measurements, urban development and on-site field interaction with people provides a practical-based theoretical model of the land characterization of an urban thermal environment which assists in regional planning and decision-making process. Various researchers have carried out extensively and successfully applied procedures and researchers on mitigating the thermal environment effects with cost-effective and environmental benefits.

As per the field verification and study found, the below-mentioned points could be applied to regional planning implications:

- It observed that the anthropogenic heat passes into the atmosphere instantly and directly. However only a few solar radiations warm up the atmosphere directly, the others are absorbed by the complex built-up concrete structures and warm up the environment indirectly. The spatial pattern and quantity of thermal emission emitted by the built-up structures, which depends on aspects (SVF) and types of building material used in construction (Memon et al., 2008). In an unplanned built-up area, substantial construction material laid within a minimal area that captures the high intensity of solar radiation. The ability of heat emitted by long-wave radiation in urban structures is significantly low this is due to low sky horizon which effects in maximum heat storage in build-up structures.
- Vegetation is a crucial factor affecting weather patterns and micro-climates. It shows the significant role in lowering the surface

Table 8
Correlation between LST over LCLU classes.

Land cover/land use	Linear regression	Coefficient of determination NDVI (R^2)
Agricultural cropland	LST = −13.054NDVI + 36.253[a]	$R^2 = 0.704$
Dense vegetation	LST = −8.3662NDVI + 34.147[a]	$R^2 = 0.422$
Sparse vegetation	LST = −29.391 NDVI + 37.959[a]	$R^2 = 0.679$
Built-up	LST = −42.888NDVI + 47.167[a]	$R^2 = 0.590$
Bare soil and exposed rocks	LST = −40.345NDVI + 47.197[a]	$R^2 = 0.260$
Scrubland and fallowland	LST = −58.122NDVI + 50.663[a]	$R^2 = 0.888$

[a] Degree Celsius.

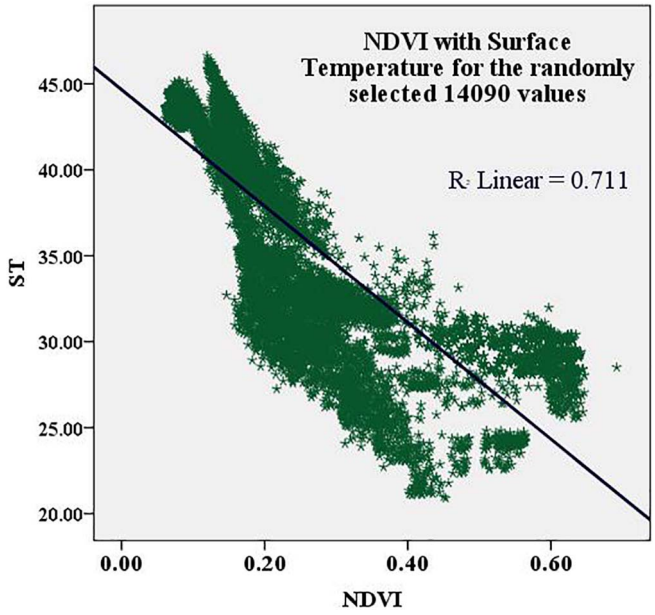

Fig. 7. Correlation between LST with NDVI.

temperature because surface structures through evapotranspiration and can reduce the amount of heat stored in the soil. Hence, lack of vegetation cover area in urban settings exhibit a low latent heat of vaporisation, but large heterogeneous building materials in urban areas decrease the amount of convective heat loss and which is also transfer by the wind. Many researchers have evaluated that urban thermal environment is negatively correlated with precipitation and wind speed while population density has a positive correlation (Mallick and Rahman, 2012). From the study, it evaluated that the land surface temperature is high where the vegetation cover found low hence, the cooling effects of vegetation provides useful guidance for planning and design of urban climate.

- Department of Environment, the Delhi Government, and concerned NGOs instigated forestation/plantations roadways sides, railway lines, along with the drains, community lands and suburban periphery. With this results, the vegetation cover of NCR Delhi increased to about 296.20 km^2 in 2009 from 26 km^2 in 1997. However, still other NCR region such as NCR Uttar Pradesh, NCR Haryana and NCR Rajasthan have not adopted such significant steps as compare to NCT Delhi, and it is also not enough forestation aligned with the increasing rate of urban growth. Regional urban planners, government bodies and NGOs should give more focus on green operations from the broader perspective.
- It observed from remote sensing imagery that trees systematically planted along with the road, water bodies, and recreational green areas show low temperatures. Therefore, it indicated the importance of trees as it mitigates the thermal effects and also recreational green areas in the urban centre. As far as concern to Yamuna River, a major tributary of river Ganges, required to be clean the river (restore), development and restoration of river bank as a biodiversity zone, reduce the point source water pollution as it polluted due to anthropogenic activity, and industrial waste. Thereby it affects water pollution and indirectly increases the temperature.
- It observed that unplanned urban built-up, as well as unauthorised colonies, inferred extreme high surface temperature (Figs. 5 and 6). Hence, by separating, planned, open space, free circulation of airspace assist in understanding the geospatial pattern of the complex thermal environment phenomena.
- For the assessment of the thermal behaviour of each LCLU classes and the thermal effect of the spatial pattern of LCLU classes, remote sensing imagery can be used efficiently to derive the geospatial information thereby it assist in planning and design of urban climate.

Identification of the areas that remain under urban thermal environment issues throughout the year, the annual urban thermal environmental map is generated for annual mean variance values. The annual variances demonstrate that most of the industrial areas, highly dense built-up areas, are under the influence of high thermal emission sites throughout the year. These areas thus need preference from urban planners to mitigate the thermal anomalies. The study performed at the regional level (viz. 46,208 km^2) using medium resolution data, but the urban thermal environmental analysis is a phenomenon that localized, and therefore it requires comprehensive study at various levels viz. administrative units, urban planning units, or beyond the land use's physical boundaries. Scale dependency is an inherent property of a geographical phenomenon, as it compared to the observation scale which could be rather than subjective depending on the observer. Therefore it is imperative to study at the observation scale using different resolutions to envisage it at the broadest sense and high-resolution levels. Moreover, the temporal variations also need to be focused in coupled with observation scale for a deeper understanding of the geographical phenomenon.

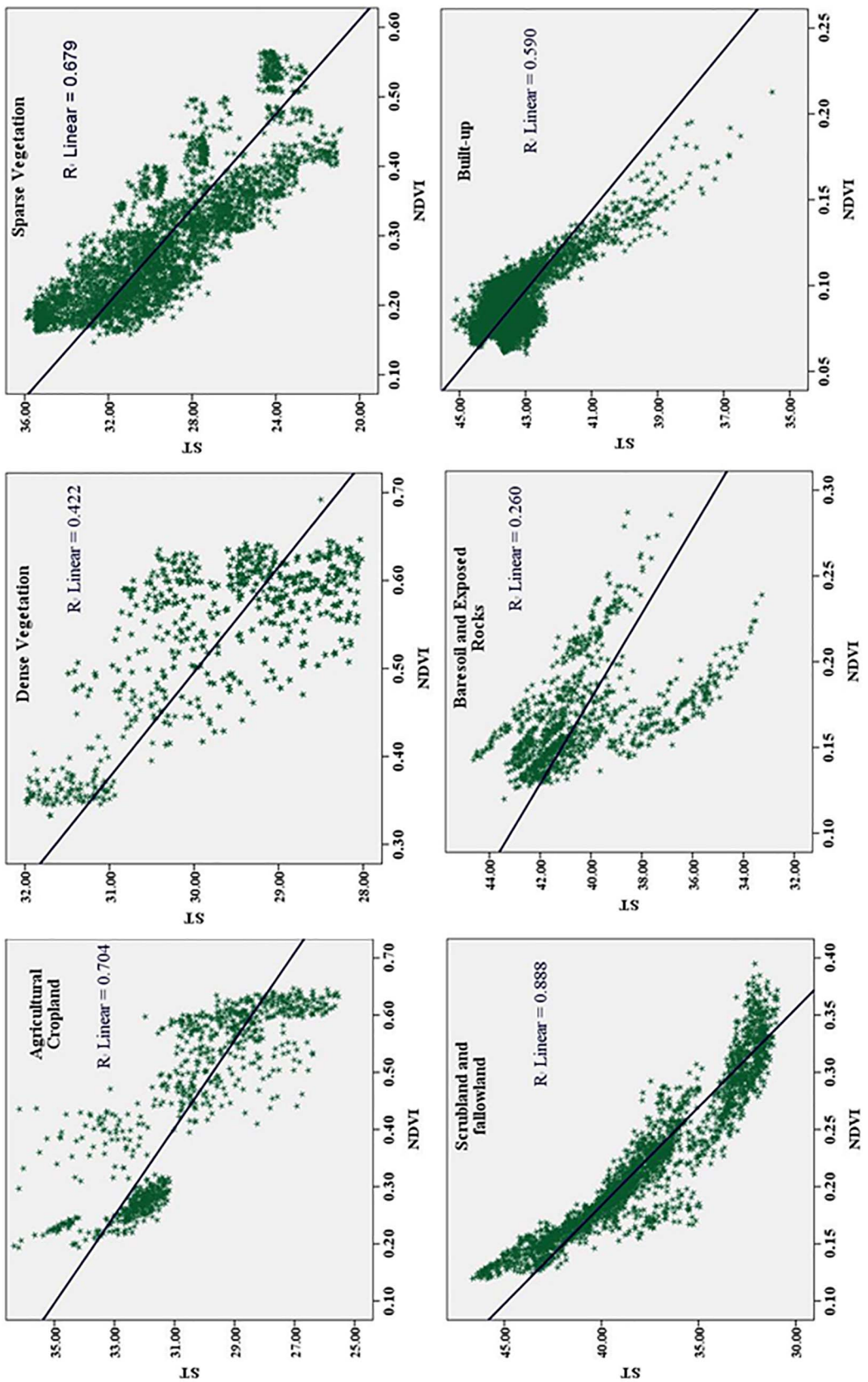

Fig. 8. LCLU class-wise correlation between LST with NDVI.

4. Conclusion

The present study is to analyse LST estimation using Landsat8 (Band 10) over NCR, India which is one of the most functionally developed regions of India. LST retrieves with the improved mono-window algorithm from the Landsat-8 Thermal Infrared Sensor Band 10. The estimation methods of ground emissivity by taking the proportion of vegetation cover coupled with Normalized Difference Vegetation Index (NDVI). Through retrieving LST of NCR, India on a warm summer day (May 2014), it found that the method used to retrieves LST were able to distinguish the surface temperature variations for different landscape surfaces. The derived ground emissivity values over different materials have also been compared with those value found in the published literature value, and it found to be in good agreement (error of around 1–2%).The comparison of LST with the field observations found in good agreement, the error of the retrieval methods of LST was about 2–3 °C. The methods were applicable for LST retrieval in the NCR, India in the hot-semi-arid environment region. The satellite-based remote sensing retrieval methods proposed and validated in the present study provide a reliable technique for observing and evaluating LST in the hot-semi-arid environment.

The visualisation of the spatial distribution of LST over various land use types within the urban areas depicted that the high densities of imperviousness (concrete structures); less porous concrete materials and frequent commercial-industrial activities contribute to the change in the micro-climatic condition of NCR, India. In the city centre area (NCT, Delhi) such as Cannought place, Chandni Chowk and its surrounding densely populated areas show the significant thermal effects, which could be visualized the spatial pattern phenomena, extent, heterogeneity, and its higher intensity of impervious cover. The impact of vegetation notified as lower temperatures over agricultural cropland, dense vegetation (forest), sparse vegetation (grass/park). The different variety of vegetation types and its canopy level showed a significantly lower surface temperature as its properties to reduce the amount of heat stored in the soil and surface structures through evapotranspiration. Pearson's correlation between vegetation density (NDVI)-surface temperature was analysed using SPSS NDVI correlated negatively with surface temperature (Pearson's correlation of -0.843) with the significant level of 0.01. Regions are having low NDVI values show the high surface temperature. The cooling effects of vegetation density on surface temperature are much stronger during summer season (May 2014) thus the surface temperature related drought indices might only be valid for the summer season. Hence, the land characterization of the urban thermal environment which is valuable parameters for regional planning and decision-making process.

Land surface temperature (LST) plays a vital role in longwave radiation estimation and energy budgets, and it has critical input criteria in climate change, hydrological, geoenvironmental models. The mono-window algorithm uses empirical equations for estimating the atmospheric transmittance and the mean temperature as the standard atmospheric profile data. However, the applicability of the algorithm is limited because the actual atmospheric conditions cannot be reflected due to use of standard atmospheric profile data. Although the estimation method of LSE by NDVI threshold method needs some improvements, it falls short to identify significant changes in the LSE, especially for barren areas. By comparing to the thermal patterns across different cities in NCR India, an appropriate methodology will be needed to extract the pattern and characterize them. Future work should focus on the application of the method to different cities of NCR India and comparison of their urban thermal behaviour.

Acknowledgement

This work is a part of PhD. Thesis under the Doctorate program at the Department of Geography, Jamia Millia Islamia, India. The authors wish to acknowledge the academic and administrative support by Deanship of Natural Sciences, Jamia Millia Islamia, India. The authors wish to thank the anonymous reviewers for their contributions to the manuscript. NASA-USGS personnel at the land DAAC provided the latest Landsat8 satellite image be also much appreciated.

References

Ali, G., Nitivattananon, V., 2012. Exercising multidisciplinary approach to assess interrelationship between energy use, carbon emission and land use change in a metropolitan city of Pakistan Renew. Sustain. Energy Rev. 16 (1), 775–786. http://dx.doi.org/10.1016/j.rser.2011.09.003.

Ali, G., Nitivattananon, V., Mehmood, H., Sabir, M., Sheikh, S.R., Abbas, S., 2012. A synthesis approach to investigate and validate carbon sources and sinks of a mega city of developing country. Environ. Dev. 4, 54–72.

Ali, G., Pumijumnong, N., Cui, S., 2017. Valuation and validation of carbon sources and sinks through land cover/use change analysis: the case of Bangkok metropolitan area. Land Use Policy 70, 471–478.

Amiri, R., Weng, Q., Alimohammadi, A., Alavipanah, S.K., 2009. The spatial–temporal dynamics of land surface temperatures in relation to fractional vegetation cover and land use/cover in the Tabriz urban area, Iran. Remote Sens. Environ. 113 (12), 2606–2617.

Anderson, J.R., Hardy, E.E., Roach, J.T., Witmer, R.E., 1976. A Land Use and Land Cover Classification System for Use with Remote Sensor Data. U. S. Geological Survey, Professional Paper 964, Reston, VA.

Buettner, K.J.K., Kern, C.D., 1965. The determination of infrared emissivities of terrestrial surfaces. J. Geophys. Res. 70, 1329–1337.

Caselles, V., Sobrino, J.A., 1989. Determination of frosts in orange groves from NOAA-9 AVHRR data. Remote Sens. Environ. 29, 135–146.

Caselles, V., Coll, C., Valor, E., 1997. Land surface emissivity and temperature determination in the whole HAPEX Sahel area from AVHRR data. Int. J. Remote Sens. 18 (5), 1009–1027.

Census of India, 2011. Provisional Population Totals, Paper 1 of 2011 India, Series-1. Office of the Registrar General & Census Commissioner, New Delhi.

Chakraborty, S.D., Kant, Y., Mitra, D., 2013. Assessment of land surface temperature and heat fluxes over Delhi using remote sensing data. J. Environ. Manag. 148, 143–152.

Chen, J.M., Zhang, R.H., 1989. Studies on the measurements of crop emissivity and sky temperature. Agric. For. Meteorol. 49, 23–34.

Chow, S.D., 1992. The urban climate of Shanghai. Atmos. Environ. 26B, 9–15.

Deng, C., Wu, C., 2013. Examining the Impacts of Urban Biophysical Compositions on Surface Urban Heat Island: A Spectral Unmixing and Thermal Mixing Approach.

Dousset, B., Gourmelon, F., 2003. Satellite multi-sensor data analysis of urban surface temperatures and landcover. ISPRS J. Photogramm. Remote Sens. 58, 43–54.

Elvidge, D., Chen, Z., 1995. Comparison of broad-band and narrow-band red and near = infrared vegetation indices. Remote Sens. Environ. 54, 38–48.

Gluch, R.Q., Saaroni, D.A., Luvall, J.C., 2006. A multi-scale approach to urban thermal analysis. Remote Sens. Environ. 104 (2), 123–132. http://dx.doi.org/10.1016/j.rse.2006.01.025.

Grimm, N.B., Faeth, S.H., Golubiewski, N.E., Redman, C.L., Wu, J., Bai, X., Briggs, J.M., 2008. Global change and the ecology of cities. Science 319, 756–760.
Husband, N.D.S., Monteith, J.L., 1986. Radiative surface temperature and energy balance of a wheat canopy.1. Comparison of radiative and aerodynamic canopy temperature. Boundary-Layer. Meteorol. Sin. 4, 106–112.
Jauregui, E., 1997. Heat island development in Mexico city. Atmos. Environ. 31, 3821–3831.
Jensen, J., 1996. Introductory Digital Image Processing. A Remote Sensing Perspective Prentice Hall, Upper Saddle River, NJ (316 pp).
Jin, Y., 1990. Emissivities of natural surfaces and surface temperature. Acta. Meteor. Sin. 4, 106–112.
Jin, M., Liang, S., 2006. An improved land surface emissivity parameter for land surface models using global remote sensing observations. J. Clim. 15, 2867–2881.
Jones, P.D., Lister, D.H., 2009. The urban heat island in central London and urban–related warming trends in Central London since 1900. Weather 64, 323–327.
Kant, Y., Badarinath, K.V.S., 2002. Ground based method for measuring thermal infrared effective emissivities: implications and perspectives on the measurement of land surface temperature from satellite data. Int. J. Remote Sens. 23 (11), 2179–2191.
Kant, Y., Bharath, B.D., Mallick, J., Atzberger, C., Kerle, N., 2009. Satellite-based analysis of the role of land use/land cover and vegetation density on surface temperature regime of Delhi, India. J. Indian Soc. Remote Sens. 37, 201–214.
Keramitsoglou, I., Kiranoudis, C.T., Ceriola, G., Weng, Q., Rajasekar, U., 2011. Identification and analysis of urban surface temperature patterns in Greater Athens, Greece, using MODIS imagery. Remote Sens. Environ. 115, 3080–3090.
Labed, J., Stoll, M.P., 1991. Spatial variability of land surface emissivity in the thermal infrared band: spectral signature and effective surface temperature. Remote Sens. Environ. 38, 1–17.
Lillesand, T.M., Kiefer, R.W., 1999. Remote Sensing and Image Interpretation. John Wiley and Sons, New York.
Liu, Y., Shintaro, G., Zhuang, D., Kuang, W., 2012. Urban surface heat fluxes infrared remote sensing inversion and their relationship with land use types. J. Geogr. Sci. 22, 699–6715.
Lo, C.P., Yeung, A.K.W., 2007. Concepts and Techniques of Geographic Information Systems (2nd Edition) (Ph Series in Geographic Information Science). Prentice-Hall, Inc., Upper Saddle River, NJ, USA ©2006 ISBN:013149502X.
Lu, D., Weng, Q., 2006. Spectral mixture analysis of ASTER imagery for examining the relationship between thermal features and biophysical descriptors in Indianapolis, Indiana. Remote Sens. Environ. 104 (2), 157–167.
Mallick, J., Rahman, A., 2012. Impact of population density on the surface temperature and micro-climate of Delhi. Curr. Sci. 102 (1708) (NO. 12).
Mallick, J., Kant, Y., Bharath, B.D., 2008. Estimation of land surface temperature over Delhi using Landsat ETM+. J. Indian Geophys. Union 12 (3), 131–140.
Mallick, J., Singh, C.K., Shashtri, S., Rahman, A., Mukherjee, S., 2012. Land surface emissivity retrieval based on moisture index from LANDSAT TM satellite data over heterogeneous surfaces of Delhi city. Int. J. Appl. Earth Obs. Geoinf. 19, 348–358.
Mallick, J., Rahman, A., Singh, C.K., 2013. Modeling urban heat islands in heterogeneous land surface and its correlation with impervious surface area by using night-time ASTER satellite data in highly urbanizing city, Delhi-India. Adv. Space Res. 52, 639–655.
Mathew, A., Sreekumar, S., Khandelwal, S., Kaul, N., Kumar, R., 2016. Prediction of surface temperatures for the assessment of urban heat island effect over Ahmedabad city using linear time series model. Energ. Buildings 128, 605–616.
Memon, R.A., Leung, D.Y.C., Chucho, L., 2008. A review on the generation, determination and mitigation of urban heat island. J. Environ. Sci. 20, 120–128.
Molla, N.A., Mollah, K.A., Ali, G., Fungladda, W., Shipin, O.V., Wongwit, W., Tomomi, H., 2012. Quantifying disease burden among climate refugees using multi-disciplinary approach: a case of Dhaka, Bangladesh. Urban Climate 8, 126–137.
Nichol, J.E., 2005. Remote sensing of urban heat islands by day and night. Photogramm. Eng. Remote. Sens. 71 (5), 613–623.
Owe, M., Griend, A.A., 1994. Ground based measurement of surface temperature and thermal emissivity. Adv. Space Res. 14 (3), 45–48.
Pandey, P., Kumar, D., Prakash, A., Masih, J., Singh, M., Kumar, S., Jain, V.K., Kumar, K., 2012. A study of urban heat island and its association with particulate matter during winter months over Delhi. Sci. Total Environ. 414, 494–507.
Punia, M., Joshi, P.K., Porwal, M.C., 2011. Decision tree classification of land use land cover for Delhi, India. Expert Syst. Appl. 38, 5577–5583.
Qin, Z., Karnieli, A., Berliner, P., 2001. A mono-window algorithm for retrieving land surface temperature from Landsat TM data and its application to the Israel Egypt border region. Int. J. Remote Sens. 22 (18), 3719–3746.
Rahman, A., Kumar, Y., Fazal, S., Bhaskaran, S., 2011. Urbanization and quality of urban environment using remote sensing and GIS techniques in East Delhi- India. J. Geogr. Inf. Syst. 3, 61–83.
Roth, M., 2002. Effects of Cities on Local Climates. Proceedings of Workshop of IGES/APN Mega-City Project, Kitakyushu, Japan.
Rubio, E., Caselles, V., Badenas, C., 1997. Emissivity measurements of several soils and vegetation types in the 8-14μm wave band: analysis of two field methods. Remote Sens. Environ. 59, 490–521.
Saitoh, T.S., Shimada, T., Hoshi, H., 1996. Modeling and simulation of the Tokyo urban heat island. Atmos. Environ. 30 (20), 3431–3442.
Salisbury, J.W., Daria, D.M., 1992. Emissivity of terrestrial materials in the 8 to 14micro meter atmospheric window, remote sensing. Environment 42, 83–106.
Schott, J.R., Volchok, W.J., 1985. Thematic mapper thermal infrared calibration. Photogramm. Eng. Remote. Sens. 51, 1351–1357.
Shabana, Ali, G., Bashir, M.K., Ali, H., 2015. Housing valuation of different towns using the hedonic model: a case of faisalabad city, Pakistan. Habitat Int. 50, 240–249.
Sharma, R., Joshi, P.K., 2013a. Identifying seasonal heat islands in urban settings of Delhi (India) using remotely sensed data – an anomaly based approach. Urban Climate 9, 19–34.
Sharma, R., Joshi, P.K., 2013b. Monitoring urban landscape dynamics over Delhi (India) using remote sensing (1998–2011) inputs. J. Indian Soc. Remote Sens. 41, 641–650.
Sharma, R., Joshi, P.K., 2016. Mapping environmental impacts of rapid urbanisation in the National Capital Region of India using remote sensing inputs. Urban Climate 15, 70–82.
Sobrino, J., Caselles, V., Coll, C., 1993. Theoretical split window algorithms for determining the actual surface temperature. II NuovoCim. 16, 219–236.
Sokhi, B.S., Sharma, N.D., Uttarwar, P.S., 1989. Satellite remote sensing in urban sprawl mapping and monitoring e a case study of Delhi. J. Indian Soc. Remote Sens. 17 (3), 57–69.
Streutker, D.R., 2003. Satellite-measured growth of the urban heat island of Houston, Texas. Remote Sens. Environ. 85 (3), 282–289.
Sutherland, R.A., 1986. Broadband and spectral emissivities (2–18 μm) of some natural soils and vegetation. J. Atmos. Ocean. Technol. 3, 199–202.
Suzanchi, K., Ravinder, K., 2011. Land use land cover change in National Capital Region of India: a remote sensing & GIS based two decadal spatialtemporal analyses. International Conference: Spatial Thinking and Geographic Information Sciences 2011. Procedia. Soc. Behav. Sci. 21, 212–221.
United Nations, 2012. World Urbanization Prospects: The 2011 Revision. Department of Economic and Social Affairs. Population Division, UN.
Valor, E., Caselles, V., 1996. Mapping land surface emissivity from NDVI. Application to European, African and South American areas. Remote Sens. Environ. 57, 167–184.
Verein Deutscher Ingenieure, 1992. Umweltmeteorologie: Wechselwirkungzwischen Atmosphare und oberflachen- Berechnung der kurz-und langwelligen Strahlung (Environmental meteorology: interaction between atmosphere and surfaces-calculation of the short and longwave radiation). VDI Richtlinien, VDI 3789.
Wang, X., Horiguchi, I., Machimura, T., 1994. Emissivities in the window region for plant canopies and the effects of plant cover ratio and others. J. Agric. Meteor. 50, 177–183.
Weng, Q., Quattrochi, D.A., 2006. Thermal remote sensing of urban areas: an introduction to the special issue. Editorial. Remote Sens. Environ. 104, 112–119.
Weng, Q., Lu, D., Schubring, J., 2004. Estimation of land surface temperature-vegetation abundance relationship for urban heat island studies. Remote Sens. Environ. 89 (4), 467–483.
Wentz Elizabeth, A., Nelson, D., Rahman, A., Stefanov, W.L., Roy, Shoursaseni, S., 2008. Expert system classification of urban land use/cover for Delhi, India. Int. J. Remote Sens. 29 (15), 4405–4427.
Yamashita, S., Sekine, K., Shoda, M., Yamashita, K., Hara, Y., 1996. On relationships between heat island and sky view factor in the cities of Tama River basin, Japan. Atmos. Environ. 20 (4), 681–686.
Yogesh, K., Bharath, B.D., Mallick, J., Atzberger, C., Kerle, N., 2009. Satellite - based analysis of the role of land use: land cover and vegetation density on surface temperature regime of Delhi, India. J. Indian Soc. Remote Sens. 37 (2), 201–214.